

# On Flow Separation Control by Means of Flapping Wings

Kevin D. Jones\*, Motomu Nakashima†, Chris J. Bradshaw\*, Jason Papadopoulos\* and Max F. Platzer\*

\*Naval Postgraduate School, Department of Aeronautics & Astronautics  
699 Dyer Rd., Monterey, California 93943, USA  
Email: jones@nps.navy.mil, platzer@nps.navy.mil

†Tokyo Institute of Technology, Department of Mechanical & Environmental Informatics  
2-12-1, O-okayama, Meguro-ku, Tokyo, 152-8552, Japan  
Email: motomu@mei.titech.ac.jp

**Abstract**—Experimental and computational results for two configurations which benefit from flow separation control are presented. Both configurations operate at low Reynolds numbers, on the order of  $10^4$ , characterized by laminar flow, often where separation is unavoidable. The first, a flapping-wing propelled micro air vehicle (MAV), consists of a biplane pair of wings flapping in counterphase located downstream of a larger stationary wing, and it is shown that flow entrainment from the flapping wings suppresses stall over the stationary wing, greatly improving the MAV performance. This is experimentally substantiated both qualitatively and quantitatively. The second configuration, a flapping-wing hydropower generator, consists of two flapping wings arranged in a tandem configuration. Numerical results indicate that optimal performance of the device occurs in the presence of massive stall, as long as the flapping motion is properly matched to the convection of the dynamic stall vortices. For both configurations, simplified panel code and Navier-Stokes computations are presented to assist in the assessment of the major geometric and flow parameters affecting the operation of the devices.

## I. INTRODUCTION

The brilliant success of birds, insects, fish and mammals which use flapping-wing propulsion for mobility has been an inspiration to humankind for hundreds if not thousands of years. It is often believed that natural selection has led to optimized designs, however it would be naive to assume that what we see in nature are truly the best possible solutions. While the optimization inherent in any evolutionary process cannot be denied, organic constraints and initial conditions must also be considered. For example, one does not find many rotating parts in nature, and therefore it may be argued that nature did not select flapping wings over propellers, but rather propellers were excluded from the process entirely. On the other hand, there are many examples in nature of organisms whose performance greatly exceeds our best predictions. Gray's paradox and the flight of the bumble-bee are classic examples.

In this paper several configurations are investigated where the control of flow-separation, by means of wing flapping, is used to improve performance. Particular interest is given to low Reynolds number flows, where laminar flow increases the likelihood of flow separation. The first case is a flapping-wing propelled micro air vehicle (MAV) with an unconventional

design (shown in Fig. 1). The tiny MAV uses a biplane pair of flapping wings for propulsion, and a leading fixed wing to provide most of the lift. By flapping the wings in counterphase, flight in ground effect is emulated, and the model is mechanically and aerodynamically balanced, providing a more stable platform. Flow separation on the fixed wing is suppressed due to flow entrained by the flapping-wing pair yielding a virtually stall-proof vehicle. The second case is an oscillating-wing hydropower generator where a pair of fluttering wings are coupled to a friction device to extract energy from the flow (shown in Fig. 2). Numerical simulations predict that optimal performance occurs in the presence of massive stall, as long as the motion is properly matched to the convection of the dynamic stall vortices (DSVs).

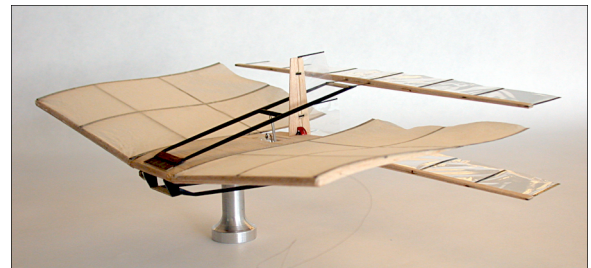


Fig. 1. Radio Controlled Flapping-Wing MAV

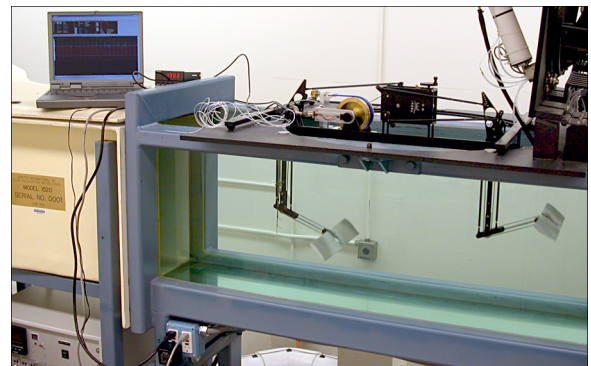


Fig. 2. Oscillating-Wing Hydropower Generator

## II. FLAPPING-WING MICRO AIR VEHICLE

The investigation of flapping-wing technologies leading to the development of the flapping-wing propelled MAVs has been underway for nearly a decade and is summarized in [1]. The radio controlled model shown in Fig. 1 has a wingspan of 27 cm, a length of 18.5 cm and weighs about 13.4 g. The fixed main wing has a span of 27 cm and a chordlength of 14.5 cm. A thin reflexed airfoil is used to provide pitch stability, and about 8 degrees of dihedral provide the necessary yaw-roll coupling. The flapping wings have a span of 25 cm and a chordlength of 4 cm, and they flap with an amplitude of about  $\pm 17$  mm. Wing pitching is enabled through a passive aeroelastic mechanism, and the minimum separation between the wings is about 5 cm.

The model is powered by a rechargeable Lithium-polymer battery with enough capacity to keep it in flight for about 15 minutes, and the radio gear provides proportional control of the throttle and rudder. With no elevator control, the model must be trimmed with a nose-up attitude, such that throttle controls the rate of climb. Flight testing of the model has shown that it will sustain flight at very high angles of attack, in excess of 15 degrees, flying at speeds below 2 m/s. When hit by gusts, the model exhibits immediate stall recovery while under power.

Recent wind-tunnel tests were used to further investigate the performance characteristics of the MAV, using a two-component force balance to directly measure lift and thrust, unsteady LDV to quantitatively investigate the surrounding flow field, and flow visualization to qualitatively assess the performance. These investigations are summarized in the following sections.

Experiments were performed in the Naval Postgraduate School low-speed wind-tunnel, a continuous, in-draft facility with a 1.5 m square test section, a 9:1 contraction ratio, and a speed range from about 0 to 9 m/s.

### A. Flow Visualization

A smoke wire was used to generate streaklines, constructed of 0.25 mm diameter NiCr beaded wire, heated by passing a current through it, and using Rosco Fog Juice as the smoke agent. Imagery was recorded using either a digital still camera or a digital video camera with a high shutter speed to freeze the motion of the wings and streaklines. Details of the methods can be found in Ref. [1].

Tests of an earlier configuration had already demonstrated the ability of the trailing, flapping wings to prevent flow separation over a leading fixed wing, as shown in Fig. 3. In the left image the wings are stationary, and the flow (moving from left to right) separates at the leading edge. In the right image the wings are flapping, and the flow appears to have reattached to the upper surface of the main wing.

For the latest series of experiments a new wind-tunnel model was fabricated which closely matched the wing geometry of the flying MAV, but which included a much larger motor, suitable for very long running times, and an optical rotary encoder to allow for direct measurements of the flapping frequency and synchronization with the LDV equipment. The

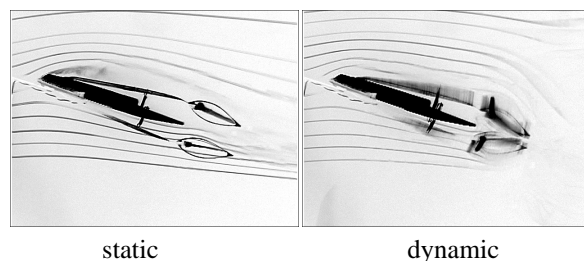


Fig. 3. Stall suppression due to flow entrainment

motor and encoder were housed in a compact fuselage, as shown in Fig. 4. Details of the model and the flow visualization experiments can be found in Ref. [2].

Flow visualization experiments were performed with the model mounted at a 15 degree angle of attack, at a flow speed of about 2 m/s, approximating the flight conditions. Initially the flapping wings were at rest, and were then quickly accelerated to a flapping frequency of about 30 Hz. The results are shown in Fig. 5, viewing the model from the left rear corner forward, an angle which provides a good view of the flow over the upper surface of the left wing. On the left, without wing flapping, it is clearly seen that the flow separates at the leading edge, and the wing is fully stalled. On the right, after just four flapping strokes, the flow is already reattached. While the boundary layer appears to be very thick and unsteady, the outer flow remains parallel to the upper wing surface and reattaches at the trailing edge. Not only is the flow entrainment sufficient to reattach the flow, but it requires only about a tenth of a second to transition. The Reynolds number is about  $2 \times 10^4$  for the main wing, and just  $5 \times 10^3$  for the flapping wings.

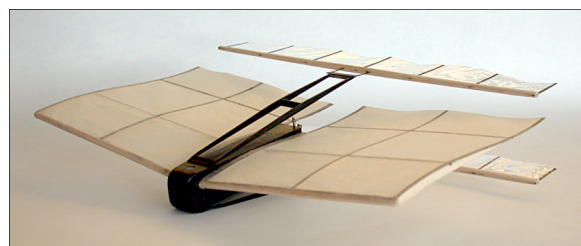


Fig. 4. Robust wind-tunnel MAV model

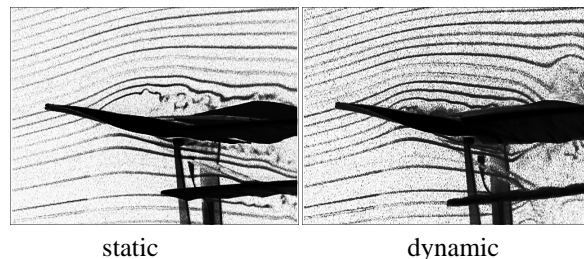


Fig. 5. Stall suppression due to flow entrainment

## B. Laser-Doppler Flow Measurements

A TSI two-channel LDV system with a single probe was used, with flow seeding provided by a Rosco fog generator. For unsteady measurements, the signal from the rotary encoder was fed into a Rotary Motion Resolver (RMR), which allowed the LDV system to record periodic data, synchronized with the wing flapping. Further details about the setup and measurement procedures can be found in [3].

Use of the RMR provided for higher fidelity velocity measurements, removing the effects of phase-biased flow seeding. Since LDV is a statistical average of a large number of recorded events, in an unsteady, periodic flow, the seeding density may fluctuate periodically, biasing the velocity prediction toward the more heavily seeded parts of the cycle.

To remedy this, using the RMR the flapping cycle was divided into 72 zones, each covering 5 degrees of the flapping cycle, and the average velocity in each zone was measured. By averaging these 72 velocities, the biasing was removed.

This is illustrated in Fig. 6 where the direct (biased) average velocity profile is compared to the average velocity profile predicted using the RMR. The velocities were recorded just downstream of the flapping wings, with the model set at a 15 degree angle of attack, flapping at 32Hz, and with a freestream velocity of 2.75 m/s. While the results are similar, measurements using the RMR tend to resolve higher peaks where flow seeding is typically more diffused.

The flow-entrainment effect is illustrated in Figs. 7 and 8. In Fig. 7 the time-averaged velocity profile just in front of the flapping wings is shown for three cases. In the first case, the main wing is removed, and the wings are flapped at 32Hz. In the second case the main wing is included, but the wings are not flapped. In the third case, the main wing is included and the wings are flapped at 32Hz. In all three cases the freestream speed is 2.75 m/s, and the model is set at a 15 degree angle of attack. Unfortunately, the dihedral of the main wing masked a large area above the symmetry plane, roughly where the figure legend is placed, such that the effect of the upper flapping wing is not visible.

Comparing the flapping cases with and without the main wing, the entrainment effect is clearly seen with about a 30 percent over-velocity at the centerline of the lower flapping wing. Note that the velocity profile is nearly un-affected by the inclusion of the main wing. Without flapping the wings, a large velocity deficit is seen near the stagnation point on the leading edge of the lower flapping wing. Also note that without flapping the wings, a velocity deficit appears more than a chordlength above the main wing, illustrating the severity of the separated flow.

In Fig. 8, velocity profiles a chordlength upstream of the flapping wings are shown for the same three cases, and it can be seen that the entrainment effect has diminished considerably, indicating that the flapping wings must be quite close to the trailing edge of the main wing to capitalize on this phenomenon.

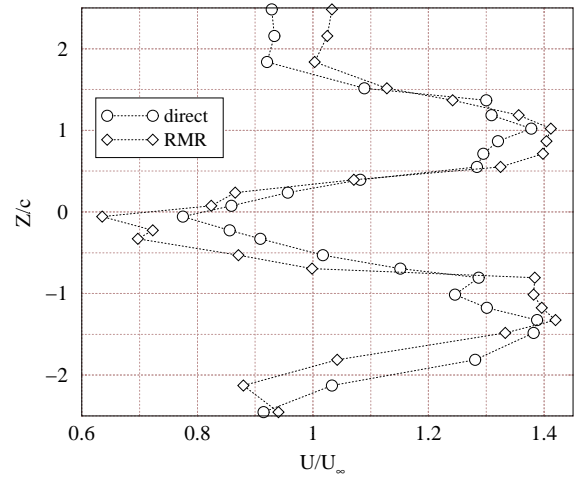


Fig. 6. Time averaging with and w/o the RMR

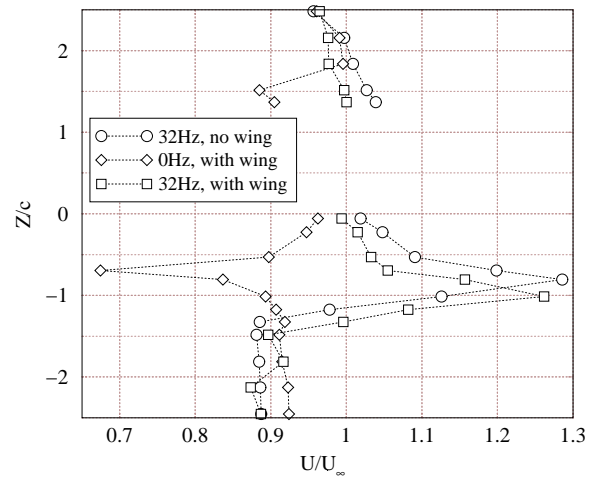


Fig. 7. Time-averaged velocity at  $x = 0$

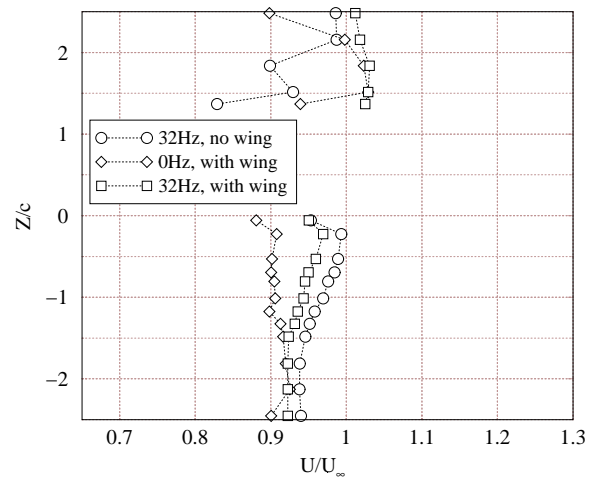


Fig. 8. Time-averaged velocity at  $x = -c$

### C. Force Measurements

Direct lift and thrust measurements were made using a two component force balance. The balance was attached to a permanent structure fixed to the concrete floor below the tunnel, preventing tunnel vibrations from degrading the results. Several configurations were evaluated over a wide gamut of conditions, however just a few results are included here to illustrate the flow entrainment effect. The apparatus, measurement procedure and all results are described in [2].

The measured thrust and lift are shown in Figs. 9 and 10, respectively, for the on-design model, and for a variation where the minimum spacing between the flapping wings is reduced from 52 mm to 30 mm. The flow speed is 3 m/s, with the models at a 15 degree angle of attack, and the flap-amplitude and all other geometric parameters are the same. Changing the separation between the wings has several effects. It changes the effectiveness of the ground-effect emulation, it changes the aeroelastic behavior of the passive pitching mechanism, and it alters the relationship between the flapping wings and the boundary layer of the main wing.

While there are questions as to the cause, the effect of the change is dramatically visible in Figs. 9 and 10. By reducing the space between the wings, the thrust is significantly reduced, but the lift is significantly increased. One theory is that in the first case the flapping wings transfer momentum into the flow in the form of thrust, and in the second case the momentum is used to reattach the boundary layer, significantly increasing the lift. More work will need to be done to evaluate this phenomenon.

### D. Computational Predictions

The computational prediction of the incompressible flow over the close-coupled stationary/flapping-wing configuration of Fig. 1 is a formidable problem which has not yet been solved. Therefore, no comparisons with the above described experiments can be presented. However, simpler configurations

have been studied using either inviscid flow assumptions or two-dimensional viscous flow assumptions.

The two-dimensional, inviscid, incompressible flow past two flapping airfoils in biplane configuration has been studied quite extensively in [4] using an unsteady panel method. These computations gave important insight into the effect of plunge and pitch amplitude and frequency on the achievable thrust, as well as the dependence on other parameters, such as the phase angle between the plunge and pitch oscillation, location of the pitch axis and the spacing between the two airfoils.

Good agreement with the experiment can, of course, be expected only if the flow remains attached. Using two-dimensional Navier-Stokes codes Tuncer and Platzer [5] and Isogai *et al* [6] have started to determine the limits of inviscid flow analyses of flapping airfoils by computing the dynamic stall boundaries of flapping airfoils, i.e., the shedding of dynamic stall vortices from the airfoil leading edge. Using a Navier-Stokes code in combination with an optimization routine Tuncer and Kaya [7] have shown that single flapping airfoils generate maximum thrust in the presence of dynamic stall, albeit at the expense of reduced propulsive efficiency. It will be interesting to generalize these Navier-Stokes calculations to the case of biplane configurations. Some results to that effect have already been given in [8] and [9].

### III. OSCILLATING-WING HYDROPOWER GENERATOR

The phenomenon of wing flutter is well known to aeronautical engineers. An aircraft wing with finite bending and torsional stiffnesses may experience catastrophic flutter under certain circumstances because the wing may absorb energy from the air flow. It follows that if an airfoil is mechanically coupled in pitch and plunge it can extract energy from the flow. It is feasible to construct an oscillating-wing power generator for the purpose of extracting useful power from a flow. In 1981, McKinney and DeLaurier [10] built such a device and called it a *wingmill*. They tested it in a wind tunnel and claimed that the wingmill achieved performance levels competitive

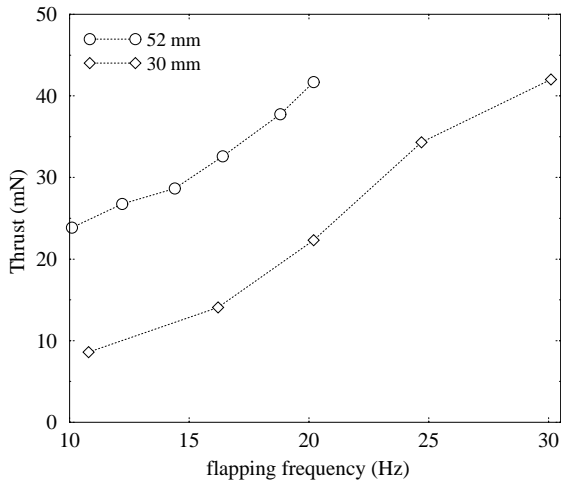


Fig. 9. Effect of wing spacing on thrust

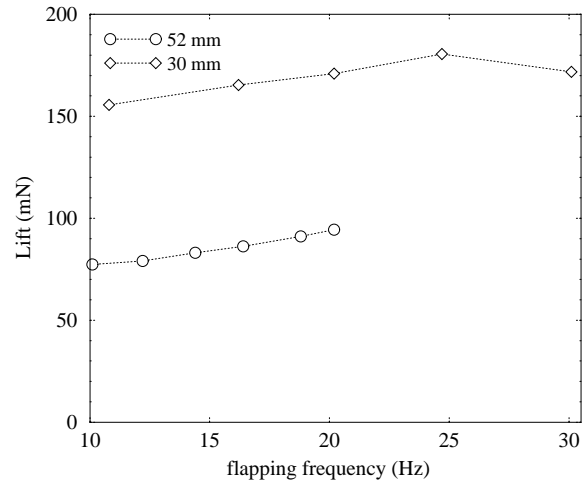


Fig. 10. Effect of wing spacing on lift

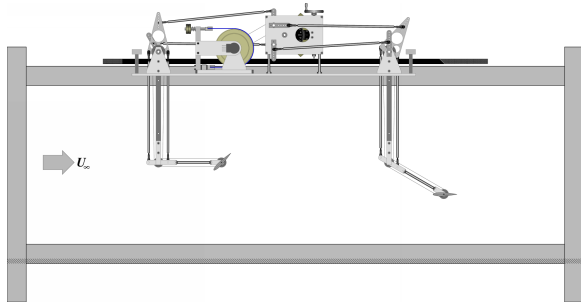


Fig. 11. Side view of the model installed in the water tunnel

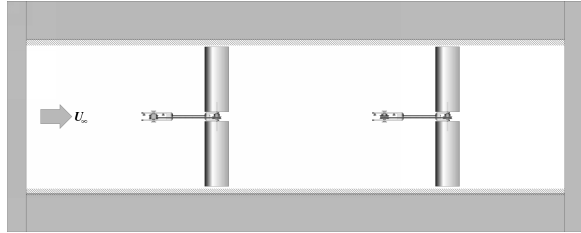


Fig. 12. Top view of the underwater components

with conventional windmills. Since their experiments, little computational or experimental work seems to have been done to further explore the potential of wingmills for power generation using either air or water flows. Water-wingmills would appear to be environmentally more acceptable than conventional hydropowerplants, especially if they can be used in slow-flowing rivers where dams are not practical due to low terrain and ship traffic. Therefore, Jones *et al* [11] and Davids [12] started to analyze the performance potential of a wingmill using a single oscillating wing and performed a first series of water tunnel tests. They concluded that the use of a single wing has considerable disadvantages which might be overcome by the use of a tandem-wing arrangement. Therefore, in [13] and [14] a tandem-wing configuration was investigated, shown previously in Figs. 2 and schematically here in 11 and 12.

#### A. Computational Predictions

Linear theory and two-dimensional panel methods may be used to rapidly predict the performance of such a device. However, in particular for a low aspect-ratio, low Reynolds number investigation, the question arises as to the accuracy of two-dimensional, inviscid methods. Therefore, three-dimensional panel simulations were run to investigate the effects of aspect ratio and the small gap between the side-by-side wing pairs, as seen in Fig. 12. The panel code is based on the method of Molino *et al* [15]. Additionally, two-dimensional Navier-Stokes simulations were run, at a Reynolds number of  $10^6$  assuming fully turbulent flow (using the Baldwin-Lomax turbulence model) and at a Reynolds number of  $2 \times 10^4$  assuming fully laminar flow, to investigate viscous flow effects. Detail of the Navier-Stokes solver can be found in [8].

The predicted power coefficients are compared in Fig. 13 for a NACA 0014 pitching about  $0.25c$  with an amplitude of

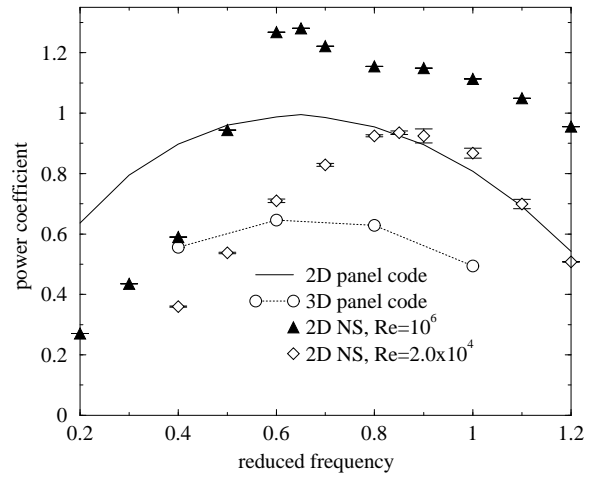


Fig. 13. Predicted power coefficient

about 73 degrees, a plunge amplitude of about  $1.3c$ , and a phase angle of 90 degrees. The three-dimensional panel code models a single wing-pair, with an aspect ratio of 2.7 and a gap between the wings of  $0.2c$ . The Navier-Stokes results include vertical error bars which indicate the standard deviation of the power over the last 3 cycles of the calculations indicating the periodicity (or lack thereof) of the solutions.

As expected, the three-dimensional losses drop the performance considerably. However, the Navier-Stokes solver, in the presence of massive separation, predicts a considerably higher power coefficient over most of the frequency range than even the two-dimensional panel code results. This indicates that separation does not hinder the performance. To the contrary, the development and convection of a large dynamic stall vortex (DSV) is critical to the high power generation. By viewing the flowfield at discrete intervals through the cycle, it is seen that at the frequency where peak power occurs ( $k \approx 0.65$ ) the DSV stays attached to the upper surface, and convects to the trailing edge at about the same time that the airfoil reaches top/bottom dead center, at which time the airfoil must rapidly change AOA. The suction provided by the DSV aids in this AOA change, and therefore increases the overall performance.

The effect of aspect ratio on the predicted lift and moment coefficients is shown in Fig. 14 for aspect ratios between 2 and 100 as well as the two-dimensional case. In this case a NACA 0014 airfoil was pitched about  $0.25c$  with an amplitude of about 68 degrees, a plunge amplitude of about  $1.3c$ , and a phase angle of 90 degrees. While the three-dimensional panel method does appear to be converging on an asymptotic solution, note however that it does not appear to be converging on the two-dimensional solution. This is also apparent in Fig. 15 where the integrated power coefficient is plotted. More work will need to be done to determine the cause of this discrepancy.

#### B. Water-Tunnel Results

The experimental model employs two wings in a tandem arrangement, as depicted in Figs. 11 and 12. The two wings

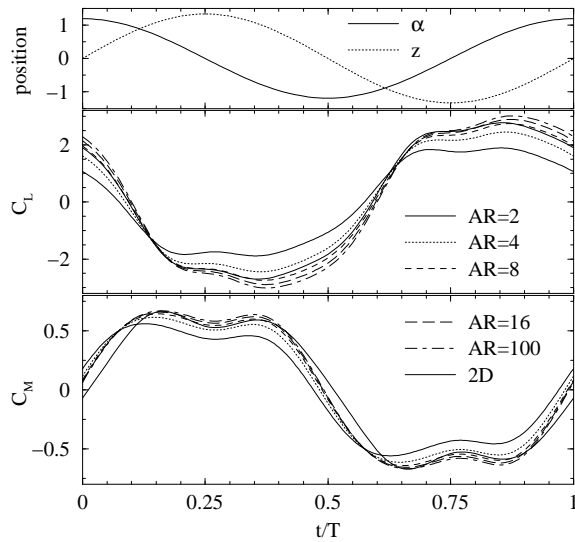


Fig. 14. Predicted effect of aspect ratio on lift and moment

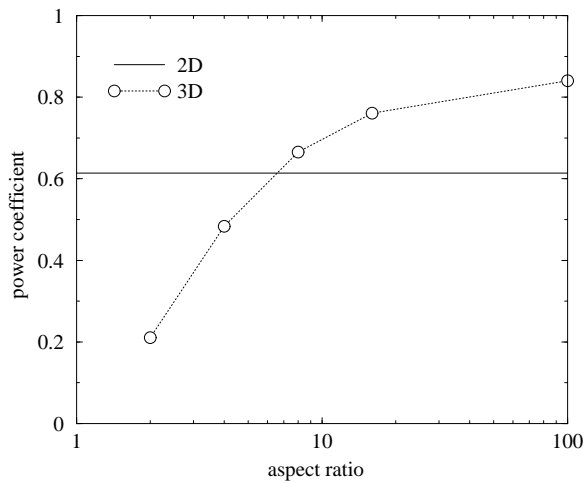


Fig. 15. Predicted effect of aspect ratio on power

have a streamwise separation of  $9.6c$ , and operate with a  $90$  degree phase difference, such that the null spot of one coincides with the power stroke of the other. Discrete pitch and plunge amplitudes and pivot locations are possible, and the phase between pitch and plunge may be varied continually during operation. The airfoil section resembles a NACA 0014, with a chord length of  $63$  mm and a half-span of  $170$  mm. Each wing assembly has two of these wing sections, separated by about  $25$ mm in the middle and about  $6$  mm clearance with the side walls. Plunge amplitudes of up to  $1.4c$ , and pitch amplitudes of up to about  $90$  degrees are possible. The model uses a Prony brake to extract power from the device.

The oscillating-wing hydropower generator was tested in the water tunnel of the Naval Postgraduate School Department of Aeronautics and Astronautics. The tunnel is a horizontal closed circuit continuous flow tunnel built by the Eidetics Corporation, capable of water velocities up to about  $0.4$  m/s.

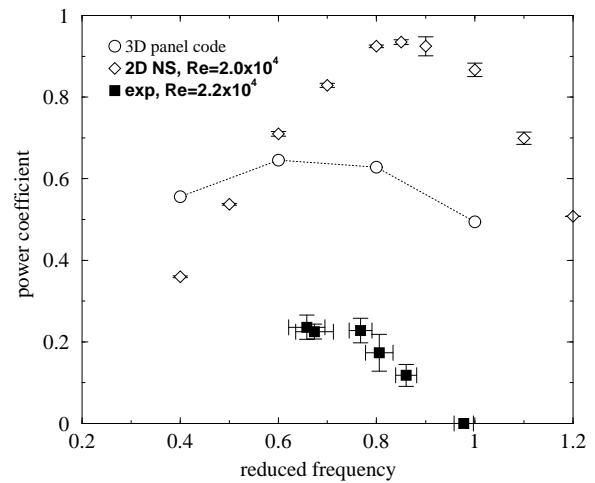


Fig. 16. Comparison of numerical and experimental results

The test section is  $38$  cm wide,  $140$  cm long, and  $50$  cm deep. At the maximum tunnel speed the Reynolds number achieved was about  $2.2 \times 10^4$ . An attempt was made to visualize the flow through the power generator by injecting dye into the water upstream of the first wing. However, at  $0.4$  m/s the rake shed a vortex street which quickly dissipated the dye making it impossible to obtain good visual flow information. Therefore, the tests were limited to obtaining measurements of the extracted power. This was accomplished by adjusting the preload tension on the Prony brake, allowing the model to operate from no-load (just overcoming friction and mechanical losses) up to the point of stall.

Data acquisition was performed using a load-cell on the Prony brake to measure torque, and a rotary encoder to determine the rotational speed. Signals from both devices were recorded on a digital storage oscilloscope (DSO) generally for a  $16$  second period. Post-processing of the two signals yielded average power and frequency and the associated deviations.

A typical set of experimental data is shown in Fig. 16, plotting the power coefficient as a function of the reduced frequency. The predictions of the three-dimensional panel code and the Navier-Stokes solver are included, and while the general trends are comparable, the magnitude of the experimental data is considerably less than the value predicted by the numerical solvers. There are many known contributors to this difference. The numerical models neglect mechanical friction, the acceleration of mechanical mass and the added mass for the submerged components, buoyancy and three-dimensional losses at the wing tips and the gap between wing sections. Additionally, the experimental wing sections are made of painted wood, and over time water was absorbed into the wood causing rather severe surface defects. Also, the trailing wing operates in the wake of the leading wing, and therefore has less energy to draw from. This tandem interference effect is not modeled in the numerics.

#### IV. CONCLUSION

Two very different flapping-wing configurations were described, both of which benefit from the control of flow separation. In the first case, flow separation on a low aspect ratio wing at a high angle of attack was suppressed due to an entrainment effect caused by a pair of flapping wings immediately downstream. The reattachment phenomenon was visualized with a smoke rake, the entrained flow was measured with LDV, and the effects on thrust and lift were measured using a force balance. Sensitivities to the location of the flapping wings were noted, but more work must be done to better understand the relationship. The phenomenon leads to a virtually stall-proof aircraft. In the second case, an oscillating-wing hydropower generator was analyzed, with numerical simulation predicting optimal performance with the flow completely separated on the suction surface, as long as the flapping motion is appropriately set to match the convection of the dynamic stall vortices.

#### REFERENCES

- [1] K. D. Jones and M. F. Platzer, "Experimental investigation of the aerodynamic characteristics of flapping-wing micro air vehicles," in *41st Aerospace Sciences Meeting & Exhibit*. AIAA Paper No. 2003-0418, Jan. 2003.
- [2] J. P. Papadopoulos, "An experimental investigation of the geometric characteristics of flapping-wing propulsion for a micro air vehicle," M.S. thesis, Department of Aeronautics & Astronautics, Naval Postgraduate School, June 2003.
- [3] C. J. Bradshaw, "An experimental investigation of flapping wing aerodynamics in micro air vehicles," M.S. thesis, Department of Aeronautics & Astronautics, Naval Postgraduate School, June 2003.
- [4] K. D. Jones and M. F. Platzer, "An experimental and numerical investigation of flapping-wing propulsion," in *37th Aerospace Sciences Meeting & Exhibit*. AIAA Paper No. 99-0995, Jan. 1999.
- [5] I. H. Tuncer and M. F. Platzer, "Computational study of flapping airfoil aerodynamics," *AIAA Journal of Aircraft*, vol. 35, no. 4, pp. 554–560, 2000.
- [6] K. Isogai, Y. Shinmoto, and Y. Watanabe, "Effects of dynamic stall on propulsive efficiency and thrust of a flapping airfoil," *AIAA Journal*, vol. 37, no. 10, pp. 1145–1151, 2000.
- [7] I. H. Tuncer and M. Kaya, "Optimization of flapping airfoils for maximum thrust," in *41st Aerospace Sciences Meeting & Exhibit*. AIAA Paper No. 2003-0420, Jan. 2003.
- [8] B. M. Castro, *Multi-Block Parallel Navier-Stokes Simulations of Unsteady Wind Tunnel and Ground Interference Effects*, Ph.D. thesis, Department of Aeronautics & Astronautics, Naval Postgraduate School, Sept. 2001.
- [9] K. D. Jones, B. M. Castro, O. Mahmoud, and M. F. Platzer, "A numerical and experimental investigation of flapping-wing propulsion in ground effect," in *40th Aerospace Sciences Meeting & Exhibit*. AIAA Paper No. 2002-0866, Jan. 2002.
- [10] W. McKinney and J. DeLaurier, "The wingmill: An oscillating-wing windmill," *Journal of Energy*, vol. 5, no. 2, pp. 109–115, 1981.
- [11] K. D. Jones and S. T. Davids and M. F. Platzer, "Oscillating-wing power generation," in *proceedings of the 3rd ASME/JSME Joint Fluids Engineering Conference*, July 1999.
- [12] S. T. Davids, "A computational and experimental investigation of a flutter generator," M.S. thesis, Department of Aeronautics & Astronautics, Naval Postgraduate School, June 1999.
- [13] K. Lindsey, "A feasibility study of oscillating-wing power generators," M.S. thesis, Department of Aeronautics & Astronautics, Naval Postgraduate School, Sept. 2002.
- [14] K. D. Jones, K. Lindsey, and M. F. Platzer, "An investigation of the fluid-structure interaction in an oscillating-wing micro-hydropower generator," in *Fluid Structure Interaction II*, S. K. Chakrabarti, C. A. Brebbia, D. Almorza, and R. Gonzalez-Palma, Eds., vol. 36 of *Advances in Fluid Mechanics*, pp. 73–82. WITPress, 2003.
- [15] L. Molino, L. Chen, and O. Suci, "Steady and oscillatory subsonic and supersonic aerodynamics around complex configurations," *AIAA Journal*, vol. 13, no. 3, pp. 368–374, 1975.